Journal of Alloys and Compounds 647 (2015) 179–188

Contents lists available at ScienceDirect

Journal of Alloys and Compounds

journal homepage: http://www.elsevier.com/locate/jalcom

Oxidation resistance and characterization of (AlCrMoTaTi)-Si_x-N coating deposited via magnetron sputtering

Du-Cheng Tsai [a], Min-Jen Deng [a], Zue-Chin Chang [b], Bing-Hau Kuo [a], Erh-Chiang Chen [a], Shou-Yi Chang [a], Fuh-Sheng Shieu [a, *]

[a] Department of Materials Science and Engineering, National Chung Hsing University, Taichung 40227, Taiwan
[b] Department of Mechanical Engineering, National Chin-Yi University of Technology, Taichung 411, Taiwan

ARTICLE INFO

Article history:
Received 31 January 2015
Received in revised form
1 June 2015
Accepted 2 June 2015
Available online 15 June 2015

Keywords:
Coating materials
Nitride materials
Vapor deposition
Crystal structure
Transmission electron microscopy
TEM

ABSTRACT

Various (AlCrMoTaTi)-Si_x-N coatings were prepared on Si substrates through a reactive magnetron sputtering system to methodically investigate the effects of Si contents and free Si on oxidation behavior. The as-deposited Si-containing coating presented a relatively dense and compact structure compared with the Si-free coating. An oxide layer was formed on the coating surface and continued to thicken when the coatings were exposed to ambient air at elevated temperatures. At 1073 K, a two-layer structure, which consists of an amorphous Al_2O_3 layer with traces of other target elements followed by a rutile TiO_2 + oxide of the target element mixed zone, was developed in the oxide layer. Oxidation resistance was gradually enhanced with the continued increase in Si concentration in the coatings. At 1173 K, the coatings with Si content of as low as 7.51 at.% exhibited a single order of magnitude lower oxidation rate than that of the Si-free coating. Nanohardness measurement of the coatings further confirmed the oxidation behavior. The significantly enhanced oxidation resistance may be attributed to the presence of Al and Si in the coatings.

1. Introduction

Since the 1970s, hard coatings have been successfully used to protect materials, particularly to enhance the life of cutting tools [1]. The technological process of the production and properties of these coatings (i.e., hardness, wear, and oxidation resistance) are continuously being improved. In particular, significant amount of efforts have been devoted to decreasing the temperature at which hard coatings are formed and improving the properties of these coatings to increase their hardness and oxidation resistance. Ternary Ti–Al–N [2,3] and Ti–Si–N [4,5] systems with higher hardness values and oxidation resistances than their TiN binary counterparts have been developed. Consequently, multi-component incorporation has great potential for developing novel hard nitride coating.

Since the 1970s, hard coatings have been successfully used to protect materials, particularly to enhance the life of cutting tools [1]. The technological process of the production and the properties of these coatings (i.e., hardness, wear, and oxidation resistance) are continuously being improved. In particular, substantial efforts have been devoted to decrease the temperature at which hard coatings are formed and improve the properties of these coatings to increase their hardness and oxidation resistance. Ternary Ti–Al–N [2,3] and Ti–Si–N [4,5] systems with higher hardness and oxidation resistance values than those of their TiN binary counterparts have been developed. Consequently, multi-component incorporation presents great potential to develop novel hard nitride coatings.

High-entropy alloys (HEAs), comprising at least five principal metal elements in near-equimolar ratios, have recently received considerable attention for their potential use in various applications. HEAs demonstrate good properties (e.g., high hardness, superior wear/oxidation resistance, and good anti-corrosion attributes) attributed to their high mixing entropies and large lattice distortions caused by incorporated multiple components [6,7]. Accordingly, given the remarkable characteristics of HEAs, novel multi-element nitride, carbide, and boride coatings with interesting properties can be developed. HEAs and their nitride films can be deposited through a simple sputtering process; these films have garnered significant interest as protective coatings for their excellent physical properties. Initial studies on high-entropy nitride

* Corresponding author.
E-mail address: fsshieu@dragon.nchu.edu.tw (F.-S. Shieu).

http://dx.doi.org/10.1016/j.jallcom.2015.06.025
0925-8388/

coatings prepared by reactive magnetron sputtering, namely, FeCoNiCrCuAlMn, FeCoNiCrCuAl$_{0.5}$, FeCoNiCrCuAl$_2$, and SiNiCrTiAl nitrides [8,9], have shown that the maximum hardness attained is only 15 GPa. This low hardness may be attributed to the incorporation of non-nitride forming elements, such as Cu and Ni. Therefore, high-entropy nitride coatings with strong nitride-forming elements, such as AlCrTaTiZr [10], AlCrMoTaTi [11], TiVCrZrHf [12,13], TiHfZrVNb [14], TiZrNbHfTa [15], and AlMoNbSiTaTiVZr [16], have been developed to increase the hardness. The nitride coatings have not only shown increased hardness but also presented a single NaCl-type phase. The TiVCrZrY nitride coating was reported to exhibit low hardness [17,18]. The softening may be related to the poor crystallinity caused by the addition of large-sized Y atoms. The Si effect of equimolar high-entropy alloy target and Si targets on high-entropy coatings through reactive magnetron co-sputtering has been investigated. Silicon incorporation significantly increases the oxidation resistance of AlCrTaTiZr nitride coatings at the expense of its hardness [19]. The improvement in the mechanical properties of AlCrMoTaTi nitride coatings with increasing Si content has also been substantiated [20].

In the current study, (AlCrMoTaTi)-Si$_x$-N coatings were deposited via reactive radio-frequency (RF) magnetron co-sputtering by using AlCrMoTaTi and Si targets. Previous research has investigated the structural evolution and the mechanical and electrical properties of (AlCrMoTaTi)-Si$_x$-N coatings [20]. However, the oxidation behavior of these coatings remains inadequately explored. The oxidation behavior of these hard coatings plays an important role in tool applications because these coatings, which are resistant to wear and corrosion, are frequently exposed to oxidative atmosphere at high temperatures. Given the promising properties of high-entropy nitrides, investigating their oxide counterparts is interesting. To our knowledge, the incorporation of Al atoms with nitrides can significantly increase the oxidation resistance of nitride coatings because the dense Al_2O_3 surface layer formed at high temperatures can effectively protect the inner unreacted coating [21]. Cr induces a similar effect of forming protective Cr_2O_3 surface layer at high temperatures [22]. The addition of Ta can decrease the number of oxygen vacancies in the surface oxide layer, thereby slowing the diffusion of oxygen [23]. Moreover, alloying Si promotes the formation of nanocomposite structure, thus obstructing oxygen diffusion along the grain boundaries [24]. Accordingly, the high oxidation resistance of (AlCrMoTaTi)-Si$_x$-N coatings should be expected. The present study explored the oxidation behavior and structural evolution of these coatings. Microstructural observation, compositional determination, and mechanical measurements were performed after the (AlCrMoTaTi)-Si$_x$-N coatings were annealed in air at different temperatures.

2. Experimental

Si$_x$(AlCrMoTaTi)$_{1-x}$N coatings were fabricated in a high-vacuum dual-target sputter deposition system with RF magnetron sputtering onto a p-type Si(100) substrate by using a 75 mm-diameter equimolar AlCrTaTiMo and Si targets. Prior to deposition, p-Si (100) wafers were cleansed in an ultrasonic bath, thoroughly rinsed with ethanol and distilled water, and then placed in a vacuum system. During the dual-target sputter deposition, the distance of the target to the substrate was 90 mm, and the deposition angle was 45° relative to the substrate. The Si substrates were cleansed and rinsed with ethanol and distilled water in an ultrasonic bath prior to deposition. The sputtering chamber was pumped to 2.67×10^{-4} Pa with a turbo pump. The flow rates of Ar and N_2 were maintained at 40 and 10 sccm, respectively. The AlCrMoTaTi target power was 150 W, with the Si target power ranging from 0 W to 180 W to obtain Si$_x$(AlCrMoTaTi)$_{1-x}$ nitride coatings under different Si

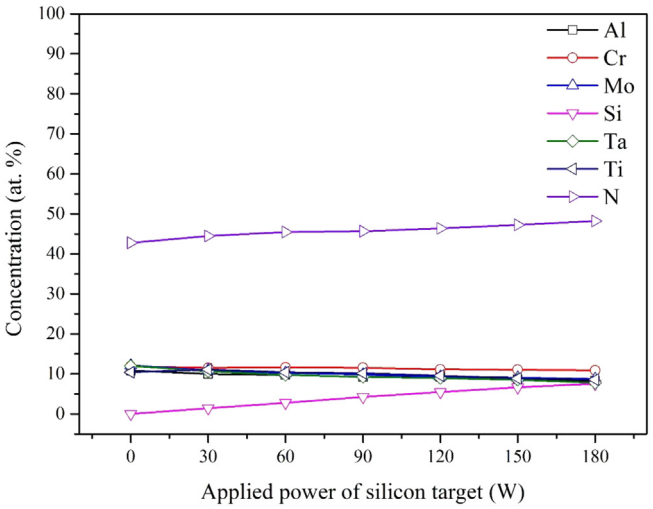

Fig. 1. EPMA element contents in nitride coatings deposited at various Si-target power.

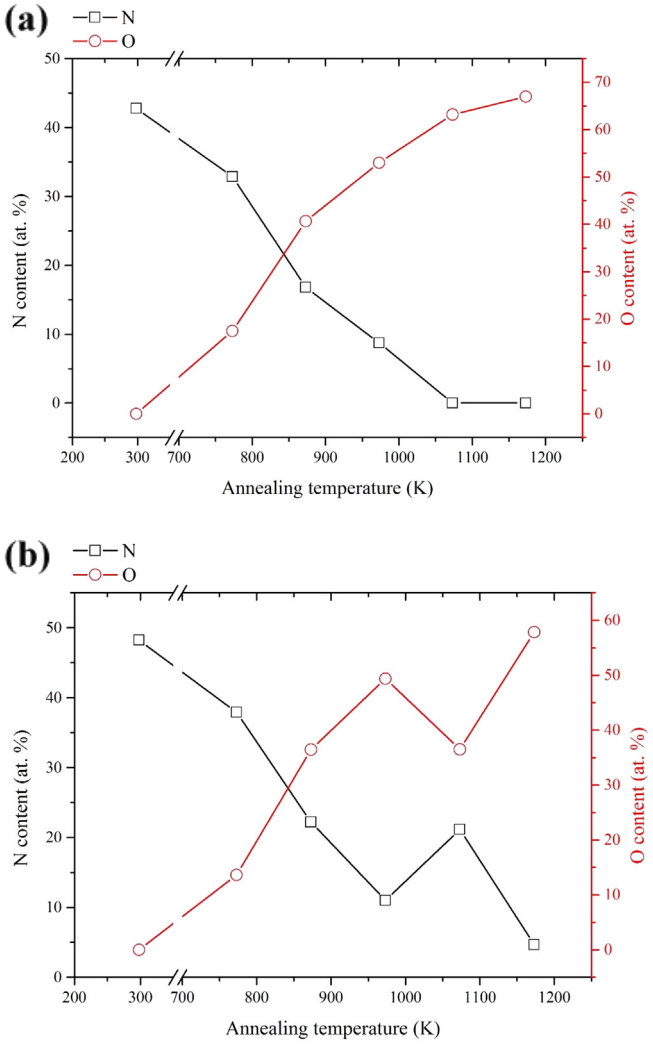

Fig. 2. FE-EPMA elemental content of the (AlCrMoTaTi)N coatings with (a) 0 at.% and (b) 7.51 at.% of Si after annealing at different temperature in air.

Table 1
The heat of formation (ΔH) of the five binary nitrides and oxides based on the target elements [27,28].

	AlN	Al_2O_3	CrN	Cr_2O_3	Mo_2N	MoO_3	TaN	Ta_2O_5	TiN	TiO_2	Si_3N_4	SiO_2
ΔH (kJ/per mole of metal element)	−318.1	−837.9	−117.2	−570.0	−35.0	−745.2	−251	−1023.0	−337.7	−944.0	−247.8	−910.7

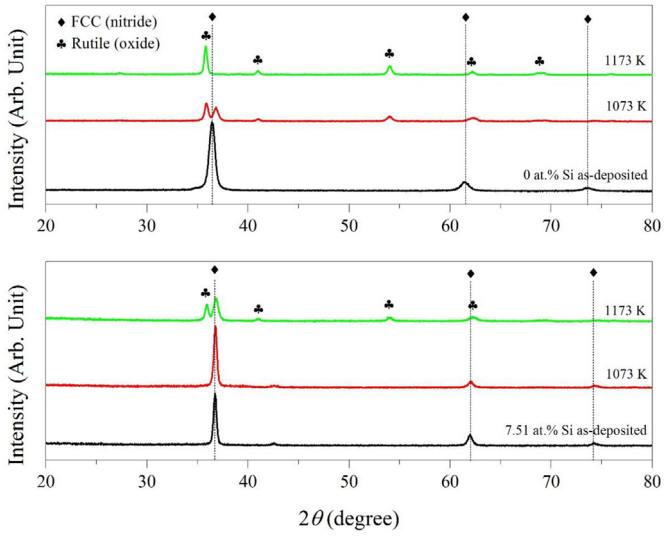

Fig. 3. X-ray diffraction pattern of the (AlCrMoTaTi)N coatings with (a) 0 at.% and (b) 7.51 at.% of Si after annealing at different temperature in air.

concentrations. The Si concentrations in the coatings increased from 0 at.% to 7.51 at.% with the increase in Si-target power [20]. The as-deposited $Si_x(AlCrMoTaTi)_{1-x}$ nitride coatings were annealed at different temperatures (773 K–1173 K) for 2 h in air by using a furnace to determine their oxidation resistance.

Variations in the coating composition, structure, and mechanical properties as a function of annealing temperature were systematically analyzed. The chemical composition of the $Si_x(AlCrMoTaTi)_{1-x}$ nitride coatings was determined using a field emission electron probe microanalysis system (EPMA, JOEL JXA-8800M). The coatings were measured in combination with the ZAF correction method [25,26] by using pure TiN and Cr_2O_3 as the reference standard materials. Given that the L spectra of Ti and Cr elements were overlapped with the K spectra of N and O elements, respectively, the spectrum deconvolution [26] approach was adopted in this study to obtain the exact composition of the coatings. The crystal structures were examined with an X-ray diffractometer (XRD, BRUKER D8 Discover) via Cu Kα radiation at a scanning speed of 1°/min. The incidence angle of the X-ray beam was set to 10°. The scanning procedure was at 0.02°, whereas the scanning range was from 20° to 80°. Morphological studies and thickness measurements were performed with a field emission scanning electron microscopy (SEM, JEOL JSM-6700F) system at an acceleration voltage of 3 kV. Microstructure and local composition

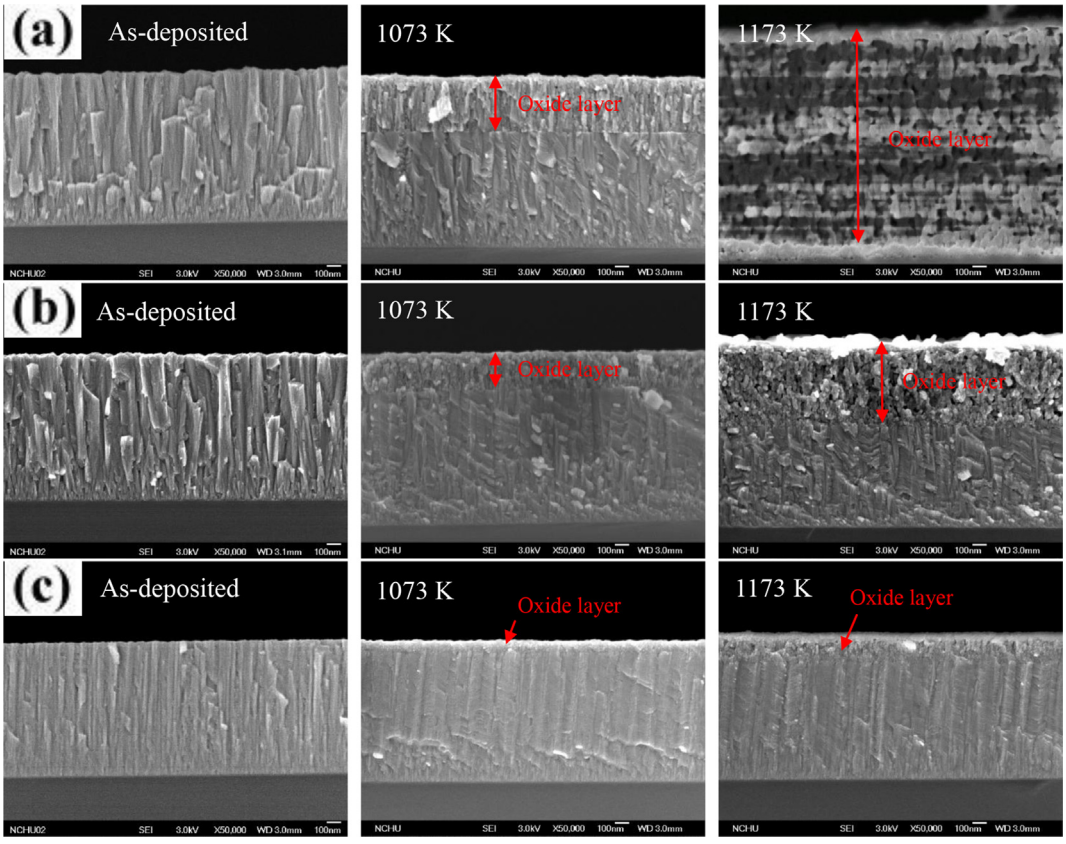

Fig. 4. Cross-sectional SEM micrographs of the (AlCrMoTaTi)N coatings with (a) 0 at.%, (b) 2.77 at.%, and (c) 7.51 at.% of Si coatings after annealing at different temperature in air.

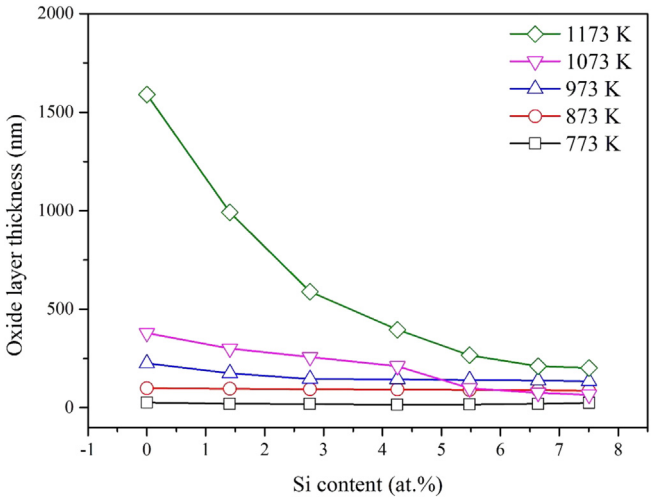

Fig. 5. Thickness of oxide layer on the top surface as a function of silicon content after annealing at different temperature in air.

were also investigated using a field emission transmission electron microscope (TEM, FEI E.O. TecnaiF20) equipped with energy-dispersive spectroscopy (EDS) at an acceleration voltage of 200 kV. The binding energy was measured by an electron spectroscopy for chemical analysis (ESCA, PHI 500 VersaProbe) with monochromatic Al Kα radiation. Nanohardness and elastic modulus of the coatings were measured with a TriboLab nanoindenter (Hysitron). At least five replicate tests were performed for each sample.

3. Results and discussion

Fig. 1 presents the EPMA-determined composition of the Si_x(-AlCrMoTaTi)$_{1-x}$N coatings prepared at various Si-target powers. The Si content in the coatings can be controlled by varying the power on the Si target. The Si content in the coatings increased linearly to 7.51 at.% with the increase in Si-target power to 180 W. Fig. 2 shows the variation of nitrogen and oxygen contents, as determined by EPMA analysis, in the (AlCrMoTaTi)N coatings with 0 and 7.51 at.% of Si, respectively, after the samples were annealed in air at different temperatures. The nitrogen content of the Si-free (AlCrMoTaTi)N coatings (Fig. 2a) evidently decreased, whereas the oxygen content increased with the increase in annealing temperature. Moreover, no nitrogen was detected, and the oxygen content was 63.2 at.% after the samples were annealed at 1073 K. These results indicated that oxygen exerts a significantly stronger tendency to react with individual metal atoms compared with nitrogen. This finding is supported by the significantly larger heat of formation of the metal oxides relative to the corresponding metal nitrides (Table 1) [27,28]. For Si-containing (AlCrMoTaTi)N coatings (Fig. 2b), the oxygen content notably increased initially with the increase in annealing temperature to 973 K and then suddenly decreased to 1073 K. This phenomenon should further be explored using other analytical instruments. The coating samples were also annealed at 1173 K, and approximately 4.7 at.% of nitrogen was still detected. The above observations indicated an evidently better oxidation resistance in the Si-containing nitride coating than in the Si-free nitride coating.

Fig. 3 illustrates the XRD patterns of the (AlCrMoTaTi)N coatings with 0 and 7.51 at.% of Si after annealing in air at different temperatures. The as-deposited nitride coating was well crystallized in an FCC structure with a strong (111) preferred orientation. However, the FCC crystal structure of the nitride coating was significantly destroyed after annealing at 1073 K. The crystalline oxide phase emerged and identified as a rutile TiO_2 structure. With further increase in annealing temperature to 1173 K, the nitride phase completely disappeared, and the oxide phase became clearer. By contrast, the Si-containing nitride coating exhibited an improved oxidation resistance during its annealing treatment in air. No other evident oxide peaks were detected, although the annealing temperature was increased up to 1073 K. The FCC solid solution nitride remained stable and constant. However, the rutile TiO_2 phase transpired after the coating was annealed at 1173 K. Similar to the EPMA observation, the addition of Si significantly contributed to the oxidation resistance of the (AlCrMoTaTi)N coating. However, the primary reason for the preferential formation of the rutile TiO_2 crystal phase remains unclear. Therefore, the current study proposes that several factors may affect the oxidation behavior of the coatings behind the air annealing of (AlCrMoTaTi)N. Table 1 demonstrates that the driving forces from nitride to oxide are different for certain elements. As a result, some elements with relatively strong oxidized tendency tend to preferentially form oxide. Moreover, some oxides with high crystallization temperature, such as Al_2O_3 and SiO_2, may be amorphous in the present case [29]; hence, they cannot be detected by XRD analysis. Ti presents a strong oxidized tendency, and its oxide exhibits low crystallization temperature [30]. In this event, the characteristic peaks of the rutile TiO_2 phase were observed in the XRD pattern. An apparent discrepancy exists in the thermal stability between the present case

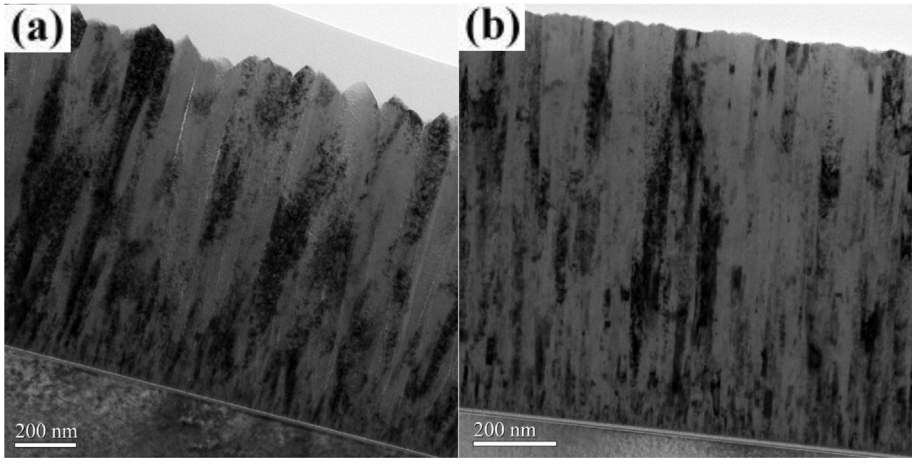

Fig. 6. Cross-sectional TEM micrographs of the as-deposited (AlCrMoTaTi)N coatings with (a) 0 at.% and (b) 7.51 at.% of Si.

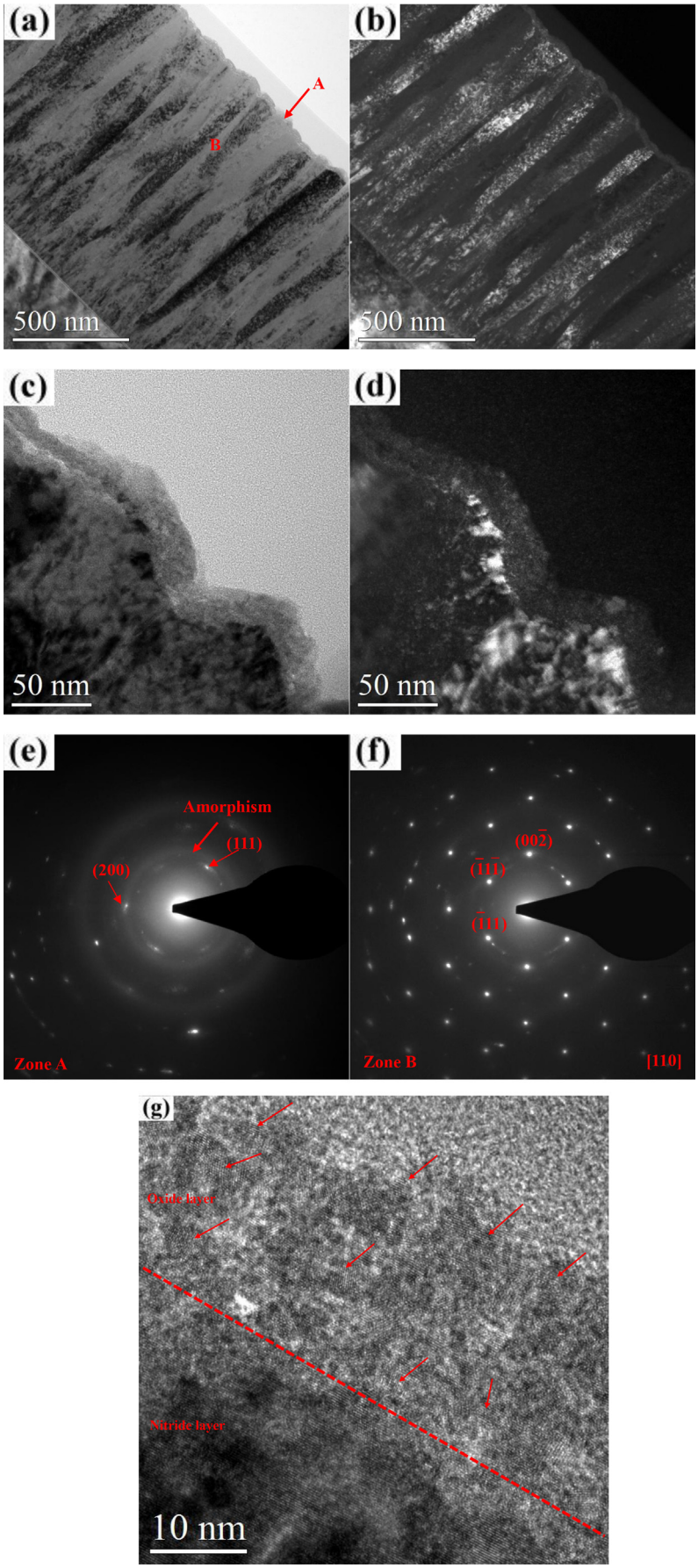

Fig. 7. Cross-sectional TEM micrographs of the (AlCrMoTaTi)N coatings after 773 K in air. (a) Bright-field image. (b) Dark-field image. (c) Higher magnification Bright-field image. (d) Higher magnification Dark-field image. (e) SAD patterns of zone A. (f) SAD patterns of zone B. (g) High resolution TEM lattice image of surface part of the cross-section.

and pure binary amorphous oxides. Such discrepancy is related to the high mixing entropy and sluggish diffusion effects on the former. The high mixing entropy effect enhances the mutual solubility among different oxides by decreasing the mixing free energy of the multi-oxide solution phase, thereby decreasing the driving force to form crystalline phases. The sluggish diffusion effect, originating from the difficulty of various atoms or ions to demonstrate cooperative diffusion, can slow down crystallization kinetics.

Further details regarding the oxides formed during the oxidation treatment can be acquired by SEM and TEM analyses. Fig. 4 reveals the SEM micrographs of the (AlCrMoTaTi)N coatings with 0, 2.77, and 7.51 at.% of Si after annealing at different temperatures in air. For the coatings without Si addition (Fig. 4a), increasing the temperature to 1073 K induced the formation of an oxide scale with a thickness of 379 nm. Further increase of the annealing temperature to 1173 K yielded a completely developed oxide scale with a thickness of 1590 nm throughout the coating. When the Si element was incorporated into the (AlCrMoTaTi)N coatings, their oxidation resistance significantly improved because the thickness of the oxide layer decreased with the increase in Si content. The dense and columnar structure of the nitride coating containing 2.77 at.% of Si (Fig. 4b) was still retained even after annealing in air at 1173 K. The oxidation at the top surface was reduced to about 589 nm. The total thickness of the oxidation layer of the nitride coating annealed at 1173 K and contains 7.51 at.% of Si (Fig. 4c) was only 202 nm, which was approximately an order of magnitude smaller than that of the

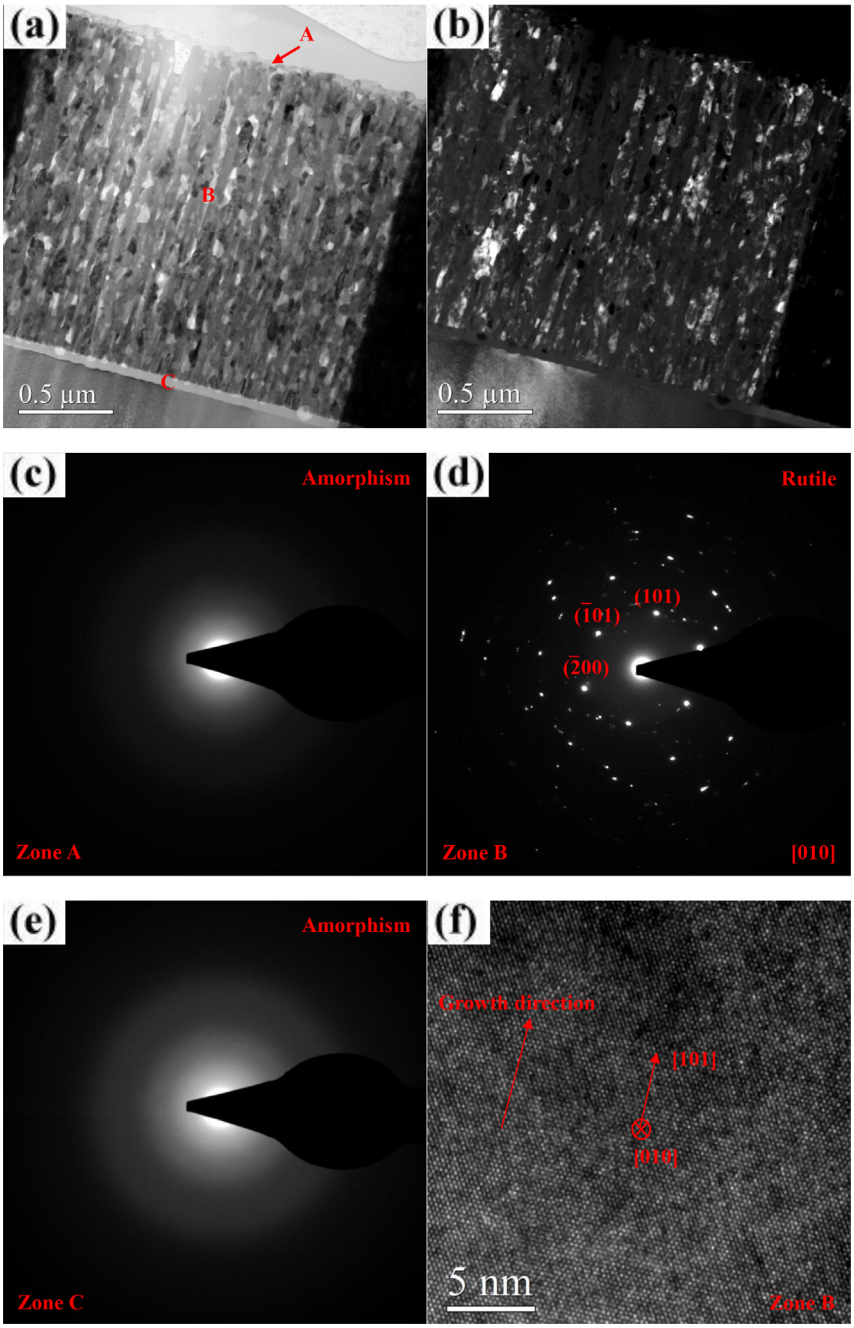

Fig. 8. Cross-sectional TEM micrographs of the (AlCrMoTaTi)N coatings after 1173 K in air. (a) Bright-field image. (b) Dark-field image. (c) SAD patterns of zone A. (d) SAD patterns of zone B. (e) SAD patterns of zone C. (f) High resolution TEM lattice image of Zone B.

Si-free nitride coating. The oxidation resistance performances of the nitride coatings with different Si contents are illustrated by SEM images in Fig. 5. The superior oxidation resistance of the Si-containing nitride coating was clearly demonstrated in this section, in which two unusual phenomena were also observed. First, two distinct layers revealed various morphologies in the oxide layer after the coating was annealed at 1073 K. Second, EPMA observation indicated that the thickness of the oxide layer was thinner after the coating was annealed at 1073 K, as opposed to when it was annealed at 973 K, in which the Si content was >5.48 at.%. Further microstructural analysis of the coating samples was conducted with TEM to understand their oxidation behavior (Figs. 6–9).

The TEM image in Fig. 6a reveals that the as-deposited nitride coating consisted of typical columns. However, significant intra- and inter-column porosities were observed in Si-free nitride. By contrast, the (AlCrMoTaTi)N coatings with 7.51 at.% of Si presented more effects and denser structure (Fig. 6b). Such denser structure eliminates the channels and poles for oxygen transport; thus, higher antioxidation properties can be expected. Fig. 7 shows the TEM images of the (AlCrMoTaTi)N coatings annealed at 773 K. A surface oxide layer (~26 nm) with visible pores was formed on the surface (Fig. 7a–d), and its composition was identified EDS spot analysis to be composed of oxygen and other target elements. The visible pores can be attributed to the nitrogen release and large volume expansion during oxidation. Two selected area diffraction (SAD) patterns of equal size were labeled as Zones A and B (Fig. 7e–f). Zone A contained weak arc-like FCC diffraction ring and a broadly diffused amorphous halo. Furthermore, Zone B revealed a large single-grain SAD pattern with an FCC structure. The combined high-resolution TEM (HRTEM) lattice image (Fig. 7g) clearly demonstrated that the oxide layer retained some nitride crystallites (shown by arrows), indicating that the oxidation process was controlled by diffusion.

Fig. 8 presents the TEM images of the (AlCrMoTaTi)N coatings annealed at 1173 K. Accordingly, the images reveal a completely developed oxide scale (~1590 nm). An extremely porous zone was observed underneath the oxidized coating (Fig. 8a–b). Three distinct layers were perceived and labeled as Zones A (Fig. 8c), B (Fig. 8d), and C (Fig. 8e). The SAD patterns of Zones A and B specify that these zones presented amorphous and rutile TiO_2 phases, respectively. The HR-TEM lattice image of Zone B (Fig. 8f) shows that the rutile TiO_2 phase exhibited highly crystalline structure with (101) preferred orientation. By measuring the chemical composition of Zone A with EDS, mostly aluminum and oxygen were identified, whereas Zone B comprised target elements and oxygen. Consequently, significant Al segregation occurred because of high temperature. The bonding states of the amorphous surface layer were further investigated by ESCA analysis. Fig. 10a shows the Al 2p photoelectron spectra, in which a binding energy of 74.7 eV was determined, corresponding to an Al–O bonding in Al_2O_3 species [31]. Fig. 10b shows the O 1s spectra, wherein the major binding energy contribution is at 531.2 eV, which are assigned to o Al–O bonding in Al_2O_3 species [31]. The above analysis confirmed that the surface layer was principally amorphous Al_2O_3. The Al

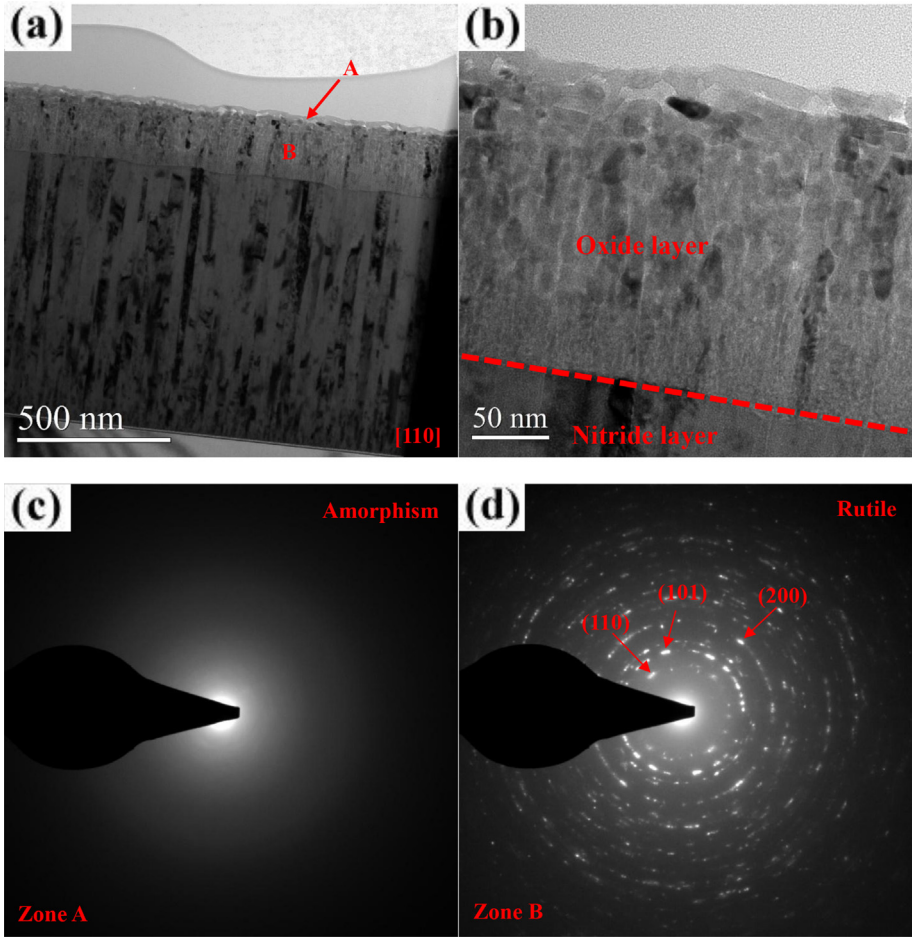

Fig. 9. Cross-sectional TEM micrographs of the (AlCrMoTaTi)N coatings with 7.51 at.% Si after 1173 K in air. (a) Bright-field image. (b) Higher magnification Bright-field image. (c) SAD patterns of zone A. (d) SAD patterns of zone B.

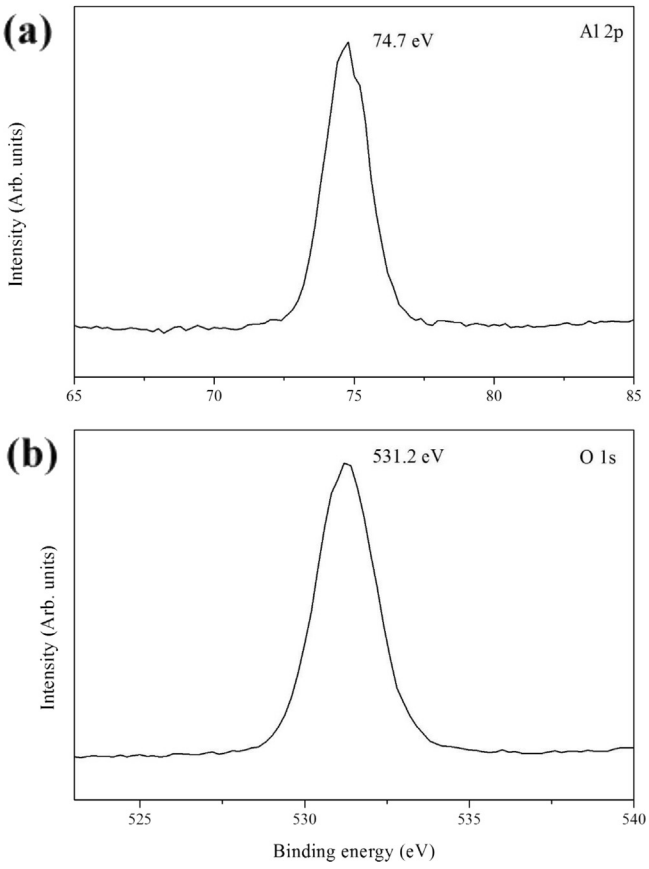

Fig. 10. ESCA spectra of (a) Al 2p and (b) O 1s for the (AlCrMoTaTi)N coatings with 7.51 at.% Si after 1173 K in air.

atoms diffused outward during oxidation and formed a stable amorphous Al_2O_3 layer at the surface region that acted as an oxygen diffusion barrier [32]. However, the high-temperature oxidation at 1173 K led to the complete failure of the Al_2O_3 barrier. The increase in oxide layer thickness during the oxidation process was accompanied by the development of stress because of the large differences of the molar volume between oxide and nitride. These stresses may induce extensive voids and may crack the protective Al_2O_3 top layer. These conditions imply that the oxygen was allowed to be freely diffuse inward through the voids and crack, intensifying the oxidation and adversely affecting the coating. Zone C was determined to be an amorphous structure in the SAD pattern (Fig. 8e). The content of the amorphous layer was determined as Si and O by EDS. The Si:O ratio was about 1:2, indicating that the interface amorphous layer was SiO_2. Obviously, the (AlCrMoTaTi)N was fully oxidized; further oxidation reaction with Si substrate continued after oxidation treatment at 1173 K. In this case, although the (AlCrMoTaTi)N coatings exhibited a better oxidation resistance than that of TiN (~823 K) [33], more effective protective coatings with good oxidation resistance should still be developed under the strict requirements of high performance and functionality.

The dense and columnar structure of nitride for the nitride coating containing 7.51 at.% of Si (Fig. 9) was retained even after its oxidation treatment at 1173 K for 2 h with added oxidation at the top surface (Fig. 9a–b). Considering the SAD observations (Fig. 9b–c), this research determined that the oxide layer was an amorphous Al_2O_3/oxide with rutile TiO_2 phase layer stack structure, similar to the (AlCrMoTaTi)N coatings annealed at 1173 K. Moreover, the findings of this study revealed that the whole thickness of the oxidized layer was only 202 nm. Accordingly, this reduced oxidation rate can be attributed to the addition of Si. The as-deposited Si containing nitride coating consists of an FCC nitride and an amorphous Si_3N_4 phase [34]. The amorphous Si_3N_4 is formed around the FCC crystallites and consequently provides a barrier to inhibit the inward diffusion of oxygen atoms through the grain boundaries. In this research, although the amorphous Si_3N_4 phase was absent, the diffused oxygen atoms may draw out the Si atoms from the solid-solution nitride and consequently form an amorphous SiO_2 phase around the crystallites because SiO_2 is immiscible with the present nitride structure. When the oxidation reaction proceeds, the oxidized SiO_2 phase exhibits a passive layer, preventing the mutual diffusion of other metallic atoms and oxidation reaction. This occurrence is a marked difference to the oxidation behavior of (AlCrMoTaTi)N. Passive layer formation is associated with a strong aluminum migration to the surface. This finding confirmed that a coating of the present alloy design effectively decreased the oxidation rate and reduced the thickness of the oxide layer. Compared with other reported nitride coatings [e.g., CrN (390 nm thick oxide layer, annealing temperature of 1073 K, holding for 4 h) [35], $Ti_{70}Si_{30}N$ (300 thick oxide layer, annealing temperature of 1123 K, holding for 1 h), and $Ti_{62}Al_{26}Si_{12}N$ (250 nm thick oxide layer, annealing temperature of 1123 K, holding for 1 h)] [36], the present coating exhibits a comparable or even superior antioxidation performance.

With the increase in Si content to 5.48 at.% and above, the nitride coating annealed at 1073 K exhibited thinner oxide layer than that annealed at 973 K. The underlying mechanism of this unusual oxidation behavior is yet to be verified. As indicated by previous analyses and discussions, Fig. 11 presents a schematic summarizing the growth of (AlCrMoTaTi)N coatings with various Si contents after annealing in air at different temperatures. The outward diffusion ability of Al increased, and the protective a-Al_2O_3 surface layer was developed at a high temperature of 1073 K. However, large stresses were produced, and the a-Al_2O_3 surface layer was cracked because of serious oxidation, thereby decreasing the protection ability from the oxygen onslaught. The addition of Si can evidently retard the oxidation rate of nitride, resulting in relatively smaller stress in coating. Briefly, the protective integrity of the a-Al_2O_3 surface layer can be maintained after the coating is annealed at 1073 K when the added Si is 5.48 at.% above. In this event, the oxidation resistance of the nitride annealed at 1073 K is better than that annealed at 973 K.

Fig. 12a and b shows the variations in the hardness and elastic modulus of (AlCrMoTaTi)N coatings with 0 and 7.51 at.% of Si after annealing in air at different temperatures. The hardness of the as-deposited (AlCrMoTaTi)N coatings was about 20.69 GPa. The hardness modulus of the coating slightly decreased with the increase in annealing temperature up to 873 K. The hardness of the coatings decreased to ~14.6 GPa after annealing at 1173 K. The coating hardness of the (AlCrMoTaTi)N coatings with 7.51 at.% of Si decreased from 35.5 GPa to 18.1 GPa but suddenly increased at 1073 K. These findings indicate that the mechanical property of the coating is associated with surface oxide layer. Oxide is envisioned to yield smaller hardness values than those of nitride. Thus, the existence of a surface oxide layer tends to reduce the hardness to values similar to those of the oxide. Moreover, given that the volume fraction of the voids in oxide layer increases with the annealing temperature in air, the mechanical properties are expected to further deteriorate.

4. Conclusion

(AlCrMoTaTi)N coating layers with various Si contents were deposited on Si substrates via reactive magnetron co-sputtering method with separate AlCrMoTaTi and Si targets. The oxidation

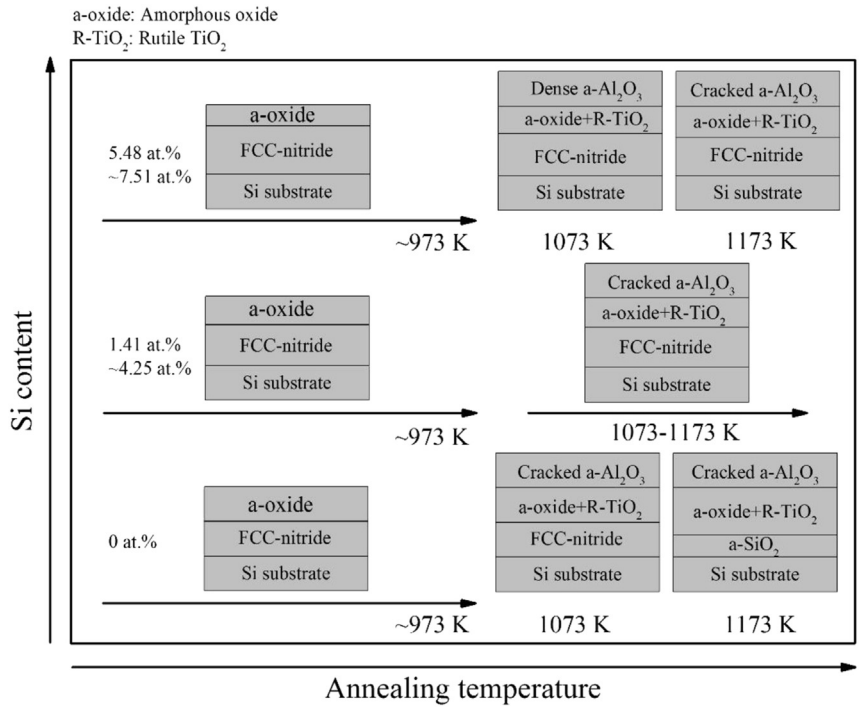

Fig. 11. The schematic diagram summarizing the growth of (AlCrMoTaTi)N coatings with different Si content after annealing in air at different temperatures.

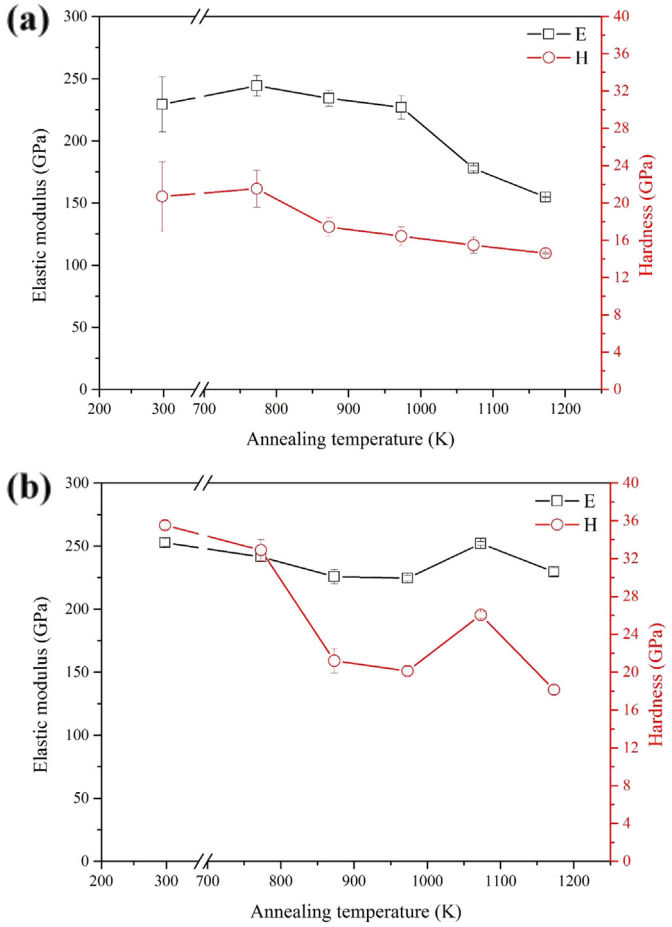

Fig. 12. Hardness and elastic modulus of the (AlCrMoTaTi)N coatings with (a) 0 at.% and (b) 7.51 at.% of Si after annealing at different temperature in air.

behavior of these coating layers at high temperatures was analyzed. Accordingly, the results indicated that the addition of Si into (AlCrMoTaTi)N coatings significantly improved the coating oxidation resistance. A silicon concentration of 7.51 at.% of Si was high enough to decrease the oxide layer thickness from 1590 nm to approximately 202 nm after oxidation at 1173 K for 2 h. The antioxidation performance of the (AlCrMoTaTi)N coatings was almost comparable or even superior to those of the T-Si-N and Ti–Al–Si–N coatings. The formed oxide scales were divided into two oxide layers. The outermost layer was amorphous Al_2O_3, which contained an extremely small amount of other target elements mainly formed by outward diffusion of Al during thermal treatment. Furthermore, the inner layer was rutile TiO_2 + oxide of the target element mixed zone. The good antioxidation performance of the coating layers may be attributed to the protective a-Al_2O_3 surface layer and a-SiO_2 phase that existed in the inner oxide layer. Accordingly, the mechanical properties of the coatings deteriorated because of the formation of an oxide layer with loose structure. The hardness of the (AlCrMoTaTi)N coatings with 7.51 at.% Si was achieved at a high level of 35.5 GPa and maintained a comparatively high value of 18.1 GPa even after annealing at 1173 K. This finding indicated that (AlCrMoTaTi)N coatings present a remarkably promising applicability for high-speed dry machining and other applications under high-temperature environments.

Acknowledgments

The authors gratefully acknowledge the financial support for this research by the Ministry of Science and Technology of Taiwan under Grant No. NSC103-2221-E-005-020-MY3. The present work was also supported in part by the Center for Micro/Nano Science and Technology of the National Cheng Kung University.

References

[1] H.O. Pierson, Handbook of Refractory Carbides and Nitrides, Noyes, New Jersey, 1996.

[2] M. Keunecke, C. Stein, K. Bewilogua, W. Koelker, D. Kassel, H. van den Berg, Modified TiAlN coatings prepared by d.c. pulsed magnetron sputtering, Surf. Coat. Technol. 205 (2010) 1273–1278.
[3] L. Chen, Y. Du, S.Q. Wang, H.H. Xu, Mechanical properties and microstructural evolution of TiN coatings alloyed with Al and Si, Mater. Sci. Eng. A 502 (2009) 139–143.
[4] Y.H. Cheng, T. Browne, B. Heckerman, E.I. Meletis, Mechanical and tribological properties of nanocomposite TiSiN coatings, Surf. Coat. Technol. 204 (2010) 2123–2129.
[5] C.K. Chung, H.C. Chang, S.C. Chang, M.W. Liao, Evolution of enhanced crystallinity and mechanical property of nanocomposite Ti–Si–N thin films using magnetron reactive co-sputtering, J. Alloys Compd. 537 (2012) 318–322.
[6] J.W. Yeh, S.K. Chen, S.J. Lin, J.Y. Gan, T.S. Chin, T.T. Shun, C.H. Tsai, S.Y. Chang, Nanostructured high-entropy alloys with multiple principal elements: novel alloy design concepts and outcomes, Adv. Eng. Mater. 6 (2004) 299–303.
[7] P.K. Huang, J.W. Yeh, T.T. Shun, S.K. Chen, Multi-principal-element alloys with improved oxidation and wear resistance for thermal spray coating, Adv. Eng. Mater. 6 (2004) 74–78.
[8] T.K. Chen, T.T. Shun, J.W. Yeh, M.S. Wong, Nanostructured nitride films of multi-element high-entropy alloys by reactive DC sputtering, Surf. Coat. Technol. 188 (2004) 193–200.
[9] T.K. Chen, M.S. Wong, T.T. Shun, J.W. Yeh, Nanostructured nitride films of multi-element high-entropy alloys by reactive DC sputtering, Surf. Coat. Technol. 200 (2005) 1361–1365.
[10] C.H. Lai, S.J. Lin, J.W. Yeh, A. Davison, Effect of substrate bias on the structure and properties of multi-element (AlCrTaTiZr)N coatings, J. Phys. D 39 (2006) 4628–4633.
[11] D.C. Tsai, Z.C. Chang, B.H. Kuo, M.H. Shiao, S.Y. Chang, F.S. Shieu, Structural morphology and characterization of (AlCrMoTaTi)N coating deposited via magnetron sputtering, Appl. Surf. Sci. 282 (2013) 789–797.
[12] D.C. Tsai, S.C. Liang, Z.C. Chang, T.N. Lin, M.H. Shiao, F.S. Shieu, Effects of substrate bias on structure and mechanical properties of (TiVCrZrHf)N coatings, Surf. Coat. Technol. 207 (2012) 293–299.
[13] S.C. Liang, Z.C. Chang, D.C. Tsai, Y.C. Lin, H.S. Sung, M.J. Deng, F.S. Shieu, Effects of substrate temperature on the structure and mechanical properties of (TiVCrZrHf)N coatings, Appl. Surf. Sci. 257 (2011) 7709–7713.
[14] A.D. Pogrebnjak, I.V. Yakushchenko, A.A. Bagdasaryan, O.V. Bondar, R. Krause-Rehberg, G. Abadias, P. Chartier, K. Oyoshi, Y. Takeda, V.M. Beresnev, Microstructure, physical and chemical properties of nanostructured (Ti-Hf-Zr-V-Nb)N coatings under different deposition conditions, Mater. Chem. Phys. 147 (2014) 1079–1091.
[15] V. Braic, Alina Vladescu, M. Balaceanu, C.R. Luculescu, M. Braic, Nanostructured multi-element (TiZrNbHfTa)N and (TiZrNbHfTa)C hard coatings, Surf. Coat. Technol. 211 (2012) 117–121.
[16] M.H. Tsai, C.H. Lai, J.W. Yeh, J.Y. Gan, Effects of nitrogen flow ratio on the structure and properties of reactively sputtered (AlMoNbSiTaTiVZr)N_x coatings, J. Phys. D Appl. Phys. 41 (2008) 235402.
[17] D.C. Tsai, Y.L. Huang, S.R. Lin, S.C. Liang, F.S. Shieu, Effect of nitrogen flow ratios on the structure and mechanical properties of (TiVCrZrY)N coatings prepared by reactive magnetron sputtering, Appl. Surf. Sci. 257 (2010) 1361–1367.
[18] D.C. Tsai, Z.C. Chang, B.H. Kuo, M.H. Shiao, S.Y. Chang, F.S. Shieu, Structure and properties of (TiVCrZrY)N coatings prepared by energetic bombardment sputtering with different nitrogen flow ratios, Appl. Phys. A 115 (2014) 1205–1213.
[19] K.H. Cheng, C.W. Tsai, S.J. Lin, J.W. Yeh, Effects of silicon content on the structure and mechanical properties of (AlCrTaTiZr)–Si_x–N coatings by reactive RF magnetron sputtering, J. Phys. D. Appl. Phys. 44 (2011) 205405.
[20] D.C. Tsai, Z.C. Chang, B.H. Kuo, S.Y. Chang, F.S. Shieu, Effects of silicon content on the structure and properties of (AlCrMoTaTi)N coatings by reactive magnetron sputtering, J. Alloys Comp. 616 (2014) 646–651.
[21] W.D. Munz, Titanium aluminum nitride films: a new alternative to TiN coatings, J. Vac. Sci. Technol. A 4 (1986) 2717–2725.
[22] D.B. Lee, Y.D. Jang, H.S. Myung, J.G. Han, High-temperature oxidation of magnetron-sputtered Cr–N-coated steels, Thin Solid Films 506 (2006) 369–372.
[23] M. Pfeiler, C. Scheu, H. Hutter, J. Schnoller, C. Michotte, C. Mitterer, M. Kathrein, On the effect of Ta on improved oxidation resistance of Ti–Al–Ta–N coatings, J. Vac. Sci. Technol. A 27 (2009) 554–560.
[24] S. Vepřek, Conventional and new approaches towards the design of novel superhard materials, Surf. Coat. Technol. 97 (1997) 15–22.
[25] S.J.B. Reed, Electron Microprobe Analysis, second ed., Cambridge University Press, New York, 1993.
[26] J. Goldstein, D.E. Newbury, D.C. Joy, C.E. Lyman, P. Echlin, E. Lifshin, L. Sawyer, J.R. Michael, Scanning Electron Microscopy and X-ray Microanalysis, third ed., Plenum Press, New York, 2003.
[27] H.O. Pierson, Handbook of Refractory Carbides and Nitrides, Noyes Publications, Westwood, New Jersey, 1996.
[28] J.A. Dean, Lange's Handbook of Chemistry, McGraw-Hill, 1999.
[29] G.D. Wilk, R.M. Wallace, J.M. Anthony, High-κ gate dielectrics: Current status and materials properties considerations, J. Appl. Phys. 89 (2001) 5243–5275.
[30] Y. Masuda1, Y. Jinbo, K. Koumoto, Room temperature CVD of TiO_2 thin films and their electronic properties, Sci. Adv. Mater. 1 (2009) 138–143.
[31] J.F. Moulder, W.F. Stickle, P.E. Sobol, K.D. Bomben, Handbook of X-Ray Photoelectron Spectroscopy, fifth ed., Physical Electronics, Inc., Eden Prairie, 1992.
[32] D. McIntyre, J. Greene, G. Håkansson, J.-E. Sundgren, W.D. Münz, Oxidation of metastable single-phase polycrystalline $Ti_{0.5}Al_{0.5}N$ films: Kinetics and mechanisms, J. Appl. Phys. 67 (1990) 1542–1553.
[33] Q. Luo, W.M. Rainforth, W.D. Münz, Wear mechanisms of monolithic and multicomponent nitride coatings grown by combined arc etching and unbalanced magnetron sputtering, Surf. Coat. Technol. 146 (2001) 430–435.
[34] S. Veprek, S. Reiprich, L. Shizhi, Superhard nanocrystalline composite materials: The TiN/Si_3N_4 system, Appl. Phys. Lett. 66 (1995) 2640–2642.
[35] I. Milosev, H.H. Strehblow, B. Navinsek, Comparison of TiN, ZrN and CrN hard nitride coatings: electrochemical and thermal oxidation, Thin Solid Films 303 (1997) 246–254.
[36] F. Vaz, L. Rebouta, M. Andritschky, M.F. da Silva, Oxidation resistance of (Ti, Al, Si)N coatings in air, Surf. Coat. Technol. 98 (1998) 912–917.